

## Spiral waves in driven strongly coupled Yukawa systems

Sandeep Kumar\* and Amita Das

*Institute for Plasma Research, HBNI, Bhat, Gandhinagar 382428, India*

(Received 3 May 2018; published 6 June 2018)

Spiral wave formations are ubiquitous in nature. In the present paper, the excitation of spiral waves in the context of driven two-dimensional dusty plasma (Yukawa system) has been demonstrated at particle level using molecular-dynamics simulations. The interaction amidst dust particles is modeled by the Yukawa potential to take account of the shielding of dust charges by the lighter electron and ion species. The spatiotemporal evolution of these spiral waves has been characterized as a function of the frequency and amplitude of the driving force and dust neutral collisions. The effect of strong coupling has been studied, which shows that the excited spiral wave structures get clearer as the medium gets more strongly coupled. The radial propagation speed of the spiral wave is observed to remain unaltered with the coupling parameter. However, it is found to depend on the screening parameter of the dust medium and decreases when it is increased. In the crystalline phase (with screening parameter  $\kappa > 0.58$ ), the spiral wavefronts are shown to be hexagonal in shape. This shows that the radial propagation speed depends on the interparticle spacing.

DOI: [10.1103/PhysRevE.97.063202](https://doi.org/10.1103/PhysRevE.97.063202)

### I. INTRODUCTION

The spiral wave formation is typically believed to arise as an interplay of propagator and controller fields in any excitable medium [1–3]. An excitable medium by definition is a nonlinear dynamical medium permitting wave propagation by means of local coupling between its constituents. However, the medium takes a certain time before a next wave can be excited through it. There are many examples of excitable media. For instance, oscillating chemical reactions such as the Belousov-Zhabotinsky (BZ) reaction [4,5] behave in this fashion. The pathological conditions in brain and heart activities have also been modeled as an excitable medium [6,7]. There are many types of waves that can be observed in any excitable medium. For example, in one dimension we can see fronts and solitons, in two dimensions we can see curvature and spiral waves, and in three dimensions scroll waves can be observed [1]. Mathematically, the FitzHugh-Nagumo (FHN) model has been widely used to describe the spatiotemporal development of spiral waves in excitable media [8–11]. In the literature, spiral waves have also been reported for many other systems, such as liquid crystals [12], a spiral galaxy [13,14], coupled oscillators [15,16], and the spread of disease in epidemiology [17]. Recently, thermal spiral wave excitation in an incompressible fluid system has been demonstrated by Li *et al.* [18].

The propagation of spiral density waves under the influence of an external force has recently been demonstrated in the fluid simulation of a compressible dusty plasma medium [19]. The dusty plasma is essentially made up of discrete charged dust particles that are of macroscopic size compared to the lighter electron and ion species present in the medium. Dusty plasma offers a model system in which to study generic phenomena such as self-organization and transport at the particle level,

which is also of great importance for excitable media. The use of a fluid model means that one misses out on the kinetic particulate nature of the dust species. Molecular-dynamics (MD) simulations, however, offer the possibility of investigating this. The aim of this paper is to seek the excitation and dynamics of the spiral wave in a dusty plasma medium by taking discrete particle effects into consideration.

Dusty plasma is a mixture of highly charged (mostly negative) and heavy ( $10^{13}$ – $10^{14}$  times heavier than the ions) dust grains along with the lighter electron and positive ion species. A typical dust particle of micron size has approximately a  $-10000e$  electronic charge. Dusty plasma can be very well depicted by a collection of point particles that interact via the Yukawa potential (which mimics the screening due to the presence of free electrons and ions between dust species) with the following form [20]:

$$U(r) = \frac{Q^2}{4\pi\epsilon_0 r} \exp\left(-\frac{r}{\lambda_D}\right).$$

Here,  $Q$  is the charge on a typical dust particle,  $r$  is the separation between two dust particles, and  $\lambda_D$  is the Debye length of background plasma. The Yukawa system can be characterized in terms of two dimensionless parameters  $\Gamma = Q^2/4\pi\epsilon_0 a k_B T_d$  (known as the coupling parameter) and  $\kappa = a/\lambda_D$  (known as the screening parameter). Here  $T_d$  and  $a$  are the dust temperature and the Wigner-Seitz radius, respectively. A Yukawa interparticle interaction also occurs in many other systems, such as charged colloids [21,22], electrolytes [23,24], and strongly coupled electron-ion (e-i) plasmas [25,26]. Therefore, the studies carried out in this work would also suitably depict these systems.

Due to high charges on the dust grains, the dusty plasmas can be easily found in the strongly coupled state (i.e., their average electrostatic potential energy can be made comparable to or higher than the average kinetic energy of particles rather easily, and it does not require extreme conditions of

\*sandeep.kumar@ipr.res.in

temperature and/or density). Such a plasma can, therefore, have traits of a fluid or a solid depending upon where the medium lies in the  $(\Gamma, \kappa)$  plane [27]. For a given  $\kappa$ , dusty plasmas imbricate to a crystalline state when the coupling parameter  $\Gamma > \Gamma_c$ , where  $\Gamma_c$  is the critical value for crystallization. At an intermediate value of  $\Gamma$  ( $1 < \Gamma < \Gamma_c$ ), the system behaves like a complex fluid with both fluid- and solidlike traits. Hence, both longitudinal and transverse wave modes can be excited in dusty plasmas. Waves in dusty plasmas are either excited by external perturbations in the form of electric fields, or self-excited by, viz., ion drag force, thermal fluctuations, and instabilities. High-amplitude perturbations in a dusty plasma medium can lead to nonlinear propagating waves that can form solitons [28,29], shocks [30], and vortices [31,32]. There are some experiments where the medium is driven by a rotating electric field (REF) [33,34]. The REF in these experiments was operated over the entire domain of the system. In the present simulation studies, we show that by employing a rotating electric field only over a small circular patch in the system, spiral waves propagating radially outward can get excited.

The paper is organized as follows. Section II provides details of MD simulation. Section III provides numerical observations. Section IV contains our conclusion.

## II. SIMULATION DETAILS

The simulation system modeled here is a two-dimensional square box of point dust particles interacting electrostatically with each other through the Yukawa form of the interaction potential. An open-source classical MD code LAMMPS [35] has been used for the purpose of simulations. A monolayer with 28647 grains (with periodic boundary conditions) is created in a simulation box with  $L_x = L_y = 300a$  ( $-150a$  to  $150a$ ) along the  $X$  and  $Y$  directions. Here,  $a = (1/\sqrt{\pi n_d})$  is the Wigner-Seitz radius in two dimensions and  $n_d$  corresponds to the dust density for the monolayer. We have assumed [36] the dust grain mass  $m_d = 6.99 \times 10^{-13}$  Kg, charge  $Q = -11940e$  ( $e$  is an electronic charge), and  $a = 4.18 \times 10^{-4}$  m. We have also considered all particles to have equal mass and charge. The screening parameter  $\kappa$  is chosen to be 0.5, which sets the plasma Debye length in the simulation as  $\lambda_D = 8.36 \times 10^{-4}$  m. The typical interdust unscreened electric field is  $E_0 = Q/4\pi\epsilon_0 a^2 = 98.39$  V/m. The equilibrium density ( $n_{d0}$ ) of the two-dimensional (2D) dust layer is  $1.821 \times 10^6$  m $^{-2}$ . The characteristic frequency of the particles  $\omega_{pd} = (Q^2/2\pi\epsilon_0 m a^3)^{1/2} \simeq 35.84$  s $^{-1}$ , which corresponds to the dust plasma period ( $t_d$ ) to be 0.175 s. We have chosen the simulation time step as  $0.0036\omega_{pd}^{-1}$  so that phenomena occurring at the dust response time scale can be easily resolved. Results in the paper are presented in normalized units, for which distance, time, and electric field are normalized by  $a$ ,  $\omega_{pd}^{-1}$ , and  $E_0$ , respectively.

A thermodynamic equilibrium state for a given  $\Gamma$  is achieved by generating positions and velocities from the canonical ensemble using a Nose-Hoover [37,38] thermostat. After about a canonical run for  $1433\omega_{pd}^{-1}$  time, we disconnected the canonical thermostat and ran a simulation for about  $716\omega_{pd}^{-1}$  time microcanonically to test the energy conservation. After a microcanonical run, the dust monolayer achieves thermodynamic equilibrium with the desired value of  $\Gamma$ .

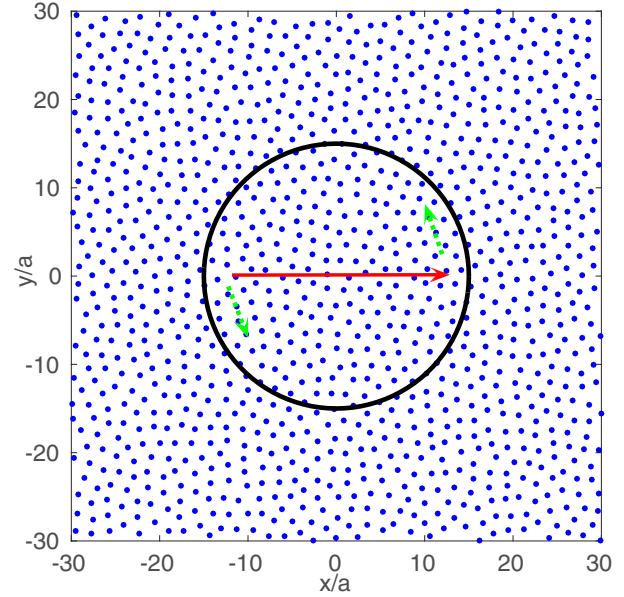


FIG. 1. Schematic representation of the circularly rotating electric field. Here, REF is only acting within the circular region on each dust particle. The absolute value of the REF is constant but rotates anticlockwise with leading time. The solid large arrow depicts the direction of REF and the small dotted arrows depict the direction of rotation.

The dust particles are then evolved in the presence of their Yukawa interactions and the external force due to the rotating electric field. The effect of background neutral gas on dust microparticles has also been studied in some simulations. For this, we have added two additional forces in the simulation. First is the neutral drag force due to the relative velocity  $\vec{v}$  between the dust grains and neutral particles, and it is given by [35,39,40]

$$\vec{F}_f = -m_d \nu \vec{v},$$

where  $m_d$  is the mass of the dust particles and  $\nu$  is the damping coefficient. The other force is random kicks suffered by dust grains by collisions with neutral atoms. This is given by

$$F_r \propto \sqrt{\frac{k_B T_n m_d \nu}{dt}},$$

where  $dt$  and  $T_n$  are the time step of simulation and background neutral gas temperature, respectively. The simulation including the effect of background neutral gas is run by Langevin MD dynamics, and the motion of the  $i$ th particle with mass  $m_d$  is governed by the following equation:

$$m_d \ddot{r}_i = - \sum_j \nabla U_{ij} + F_f + F_r + F_{\text{rot}}. \quad (1)$$

Here,  $F_{\text{rot}} = QE_{\text{rot}}$  is the force due to the REF of the form  $E_{\text{rot}} = A \cos(\omega_f t)\hat{x} + A \sin(\omega_f t)\hat{y}$ , where,  $A$  is the amplitude of the REF and  $\omega_f = 2\pi/T_f$ . It should be noted that  $F_{\text{rot}}$  is only acting on those particles that lies within the circular patch, as shown in the schematic representation of Fig. 1. For most of our simulations, unless otherwise stated, we have used the value of  $\Gamma = 100$ ,  $\kappa = 0.5$ , and  $\nu = 0$ . However, in some cases to investigate the dependence on these parameters, we have also

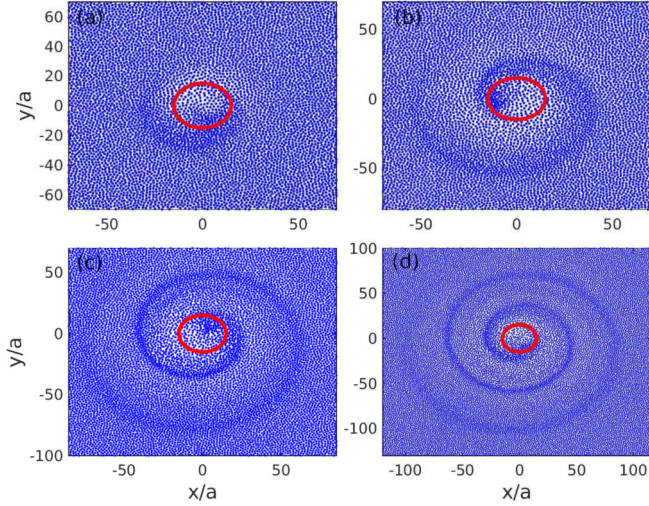


FIG. 2. Time evolution of the medium for REF of amplitude  $A = 0.203$ ,  $\omega_{pd}T_f = 26.88$ ,  $\Gamma = 100$ , and  $\kappa = 0.5$ . Particle snapshots taken at time (a)  $\omega_{pd}t = 17.92$ , (b)  $\omega_{pd}t = 35.84$ , (c)  $\omega_{pd}t = 53.76$ , and (d)  $\omega_{pd}t = 71.68$  are clearly showing the formation of a spiral wave. The circle at the center represents the region of forcing.

varied these values as per the requirement. In the simulation,  $\Gamma$  and  $\kappa$  are varied by varying  $T_d$  and  $\lambda_D$ , respectively. The characteristic dust lattice wave (DLW) velocity ( $C_s$ ) of the medium at  $\Gamma = 100$ ,  $\kappa = 0.5$ , and  $\nu = 0$  is  $1.94 \times 10^{-2}$  m/s [28].

### III. NUMERICAL OBSERVATIONS

We have applied a rotating electric field on a small circular region at the center of the two-dimensional simulation box to excite the spiral waves. In the present simulation, we have chosen the radius of circular region  $r_0 = 15a$ . A rotating electric field  $E(t)$  is generated by choosing the following time dependence for the two components, viz.,  $E_x(t) = A \cos(\omega_f t + \psi)$  and  $E_y(t) = A \sin(\omega_f t)$  along the  $X$  and  $Y$  axis, respectively. Here,  $\omega_f = 2\pi/T_f$  so that  $T_f$  is the period of rotation. The superposition  $E = (E_x, E_y)$  gives rise to a polarized electric field rotating in two dimensions. The type of polarization depends upon the phase difference ( $\Delta\phi$ ) among  $E_x$  and  $E_y$ . For linear polarization  $\Delta\phi = 0$  or  $\pi$ , circular polarization  $\Delta\phi = \pi/2$  or  $3\pi/2$  and elliptical polarization  $\Delta\phi = \pi/4$  or  $3\pi/4$ . In the present studies, the case of circular polarization has been employed. A schematic representation of REF is shown in Fig. 1. This electric field results in an electrostatic force  $F_E = QE$  on the dust particles that creates spatial perturbation in dust density ( $\vec{\nabla}n_d$ ). The forcing also imparts kinetic energy to the particles, which can randomize and create temperature gradients ( $\vec{\nabla}T_d$ ) in the medium. The applied REF has been kept on for the entire duration of simulation.

The evolution of the medium is shown in Fig. 2. Particle snapshots clearly show the excitation of the collective mode of a spiral waveform that is rotating as well as radially expanding. The handedness of the spiral motion depends upon the type of polarization (left or right circular) of the driver field. This spiral wave is a manifestation of the forcing on the dust particles by the REF, which is operative over the central circular region

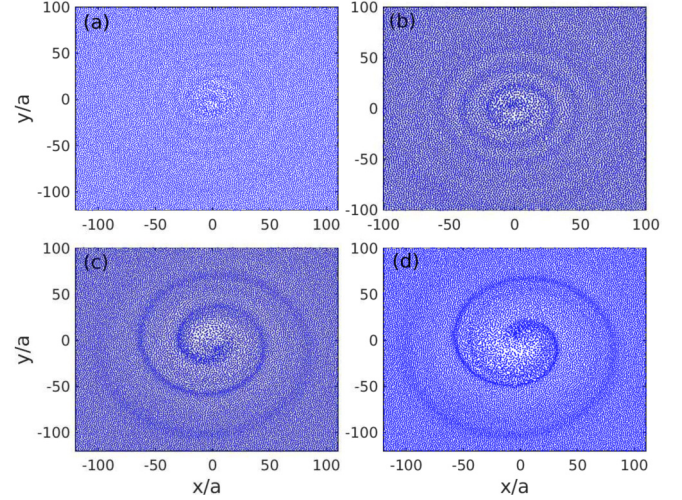


FIG. 3. Spiral waves for different values of driver frequency (a)  $\omega_{pd}T_f = 12.54$ , (b)  $\omega_{pd}T_f = 16.12$ , (c)  $\omega_{pd}T_f = 26.88$ , and (d)  $\omega_{pd}T_f = 35.84$  at  $A = 0.203$ ,  $\Gamma = 100$ , and  $\kappa = 0.5$ . Snapshots of particles for all frequencies are taken at time  $\omega_{pd}t = 71.68$ .

shown in Fig. 2 by a thick line. The number of rings in the spiral structure at a given time is proportional to the number of periods taken by the REF in that duration. In Fig. 2, the number of rings according to the number of periods from four plots (a), (b), (c), and (d) are  $17.92/26.88 = 0.67$ ,  $35.84/26.88 = 1.33$ ,  $53.76/26.88 = 2.0$ , and  $71.68/26.88 = 2.67$ , respectively, as expected. We have calculated the radial velocity of the spiral wave from the propagation of the density peak radially outward (for instance, the  $X$  axis was specifically chosen here) with respect to time. The density data as a function of  $x$  are obtained by calculating the density of particles within spatial grids along the  $X$  axis. The radial velocity for  $A = 0.203$ ,  $\omega_{pd}T_f = 26.88$ ,  $\Gamma = 100$ ,  $\kappa = 0.5$ , and  $\nu = 0$  is  $1.97 \times 10^{-2}$  m/s, which is very close to the DLW velocity ( $C_s = 1.94 \times 10^{-2}$  m/s) [28].

The number of spirals generated at a given time is a function of the frequency of the REF. With increasing frequency of the REF, the number of spiral rings increases, as shown in Figs. 3 and 4. However, since the radial expansion is governed by the acoustic propagation speed, the radial separation between two consecutive density peaks reduces with increasing frequency. At very high frequency [plot (a) of Fig. 3], the spiral density compression and rarefaction is not very clear. In this case, the radial expansion is unable to keep pace to distinctly identify the individual density peaks.

When the amplitude of the driving force is increased, the density perturbation ( $\delta n = n_d - n_{d0}$ ) in the spiral is of higher amplitude and the spiral rings are broader. This is evident from the plot of Fig. 5. Furthermore, one can observe that with increasing amplitude of force, the particles in the central region acquire higher velocities that get randomized. The consecutive rings, therefore, have varying radial speed of propagation and the spiral structure does not form clearly. Therefore, in forming a good spiral structure, the amplitude of driving force also plays a crucial role.

We have also applied frictional damping on the dust particles due to the presence of neutral particles in the dusty plasma medium. We have found that the spiral wave gets damped in the

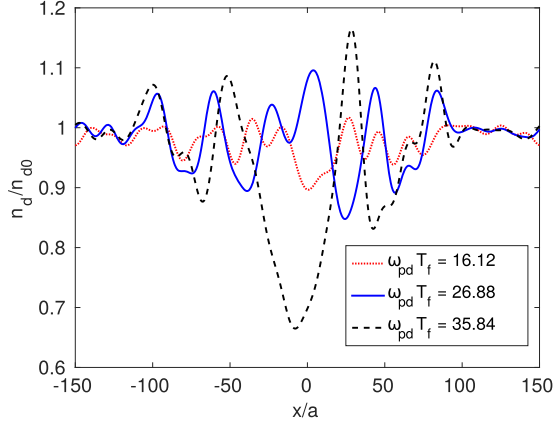


FIG. 4. One-dimensional density of the medium for the different frequencies of driver at  $A = 0.203$ ,  $\Gamma = 100$ , and  $\kappa = 0.5$ . Density plots for all frequencies are taken at time  $\omega_{pd}t = 71.68$ . From the plot it is clear that with a decrease in the frequency of the external driver, the density compression, rarefaction, and distance between two consecutive rings increases.

presence of frictional damping ( $\vec{F}_f$ ). The damping rate increases with an increase in the damping coefficient ( $\nu$ ), as shown in Fig. 6.

We have also studied the effect of  $\Gamma$  and  $\kappa$  on the formation and evolution of spiral waves. When the value of the coupling parameter ( $\Gamma$ ) of the medium is increased, one observes that spiral rings become more distinctly clear (Fig. 7). This can be understood from the fact that in the weakly coupled case, particle trajectories are diffusive, but they become localized in the strongly coupled case. Another observation is that the coupling parameter  $\Gamma$  has a negligible influence on the radial

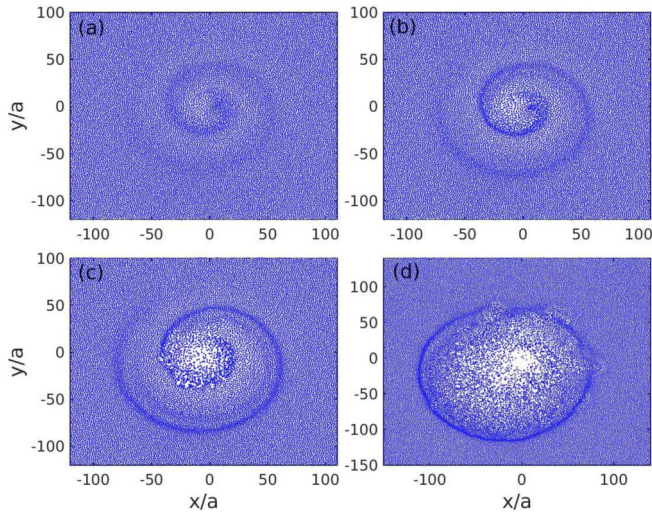


FIG. 5. Characteristics of spiral waves with varying amplitudes of REF: (a)  $A = 0.101$ , (b)  $A = 0.203$ , (c)  $A = 0.406$ , and (d)  $A = 1.27$ . The coupling parameter, screening parameter, and time period of REF for all amplitudes are  $\Gamma = 100$ ,  $\kappa = 0.5$ , and  $\omega_{pd}T_f = 26.88$ , respectively. Snapshots of particles for all amplitudes are taken at time  $\omega_{pd}t = 50.17$ . From the figure, it is clear that an undistorted (tip) spiral wave can be excited when the amplitude of REF is smaller than the interdust unscreened electric field ( $E_0$ ).

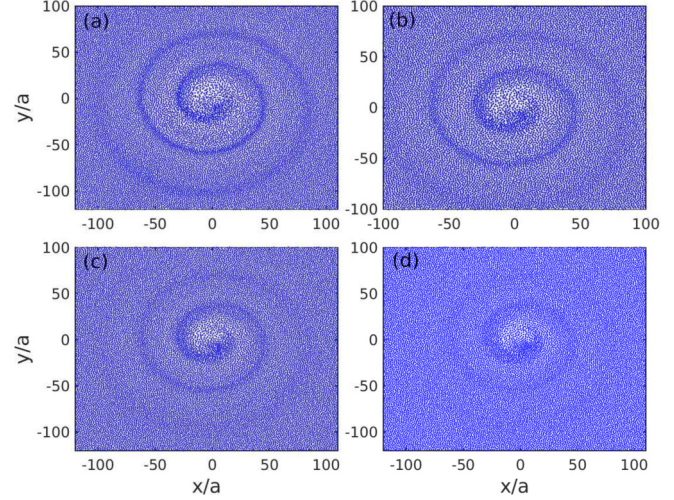


FIG. 6. The effects of neutral damping (a)  $\nu/\omega_{pd} = 0.0$ , (b)  $\nu/\omega_{pd} = 0.014$ , (c)  $\nu/\omega_{pd} = 0.0279$ , and (d)  $\nu/\omega_{pd} = 0.0558$  on the spiral wave are shown here. For all the plots,  $A = 0.203$ ,  $\omega_{pd}T_f = 26.88$ ,  $\Gamma = 100$ , and  $\kappa = 0.5$ . Snapshots of particles for all damping parameters are taken at time  $\omega_{pd}t = 71.68$ .

propagation speed of the spiral wave. The screening parameter  $\kappa$ , however, has a strong effect. The radial propagation velocity decreases with an increase in the value of  $\kappa$ . The role of  $\Gamma$  and  $\kappa$  parameters has been illustrated in the plots (a), (b), (c), and (d) of Figs. 7 and 8, respectively. The dependency of the radial velocity of the spiral on  $\Gamma$  and  $\kappa$  is also in accordance with the findings of Khrapak *et al.* [42] and Kalman *et al.* [43] obtained for the sound velocity of strongly coupled Yukawa liquids. Kalman *et al.* suggested that an approximate expression for the sound velocity of the Yukawa liquids valid for  $\kappa < 2.5$  is as follows:

$$C_s = \omega_{pd}a\sqrt{[1/\kappa^2 + f(\kappa)]}, \quad (2)$$

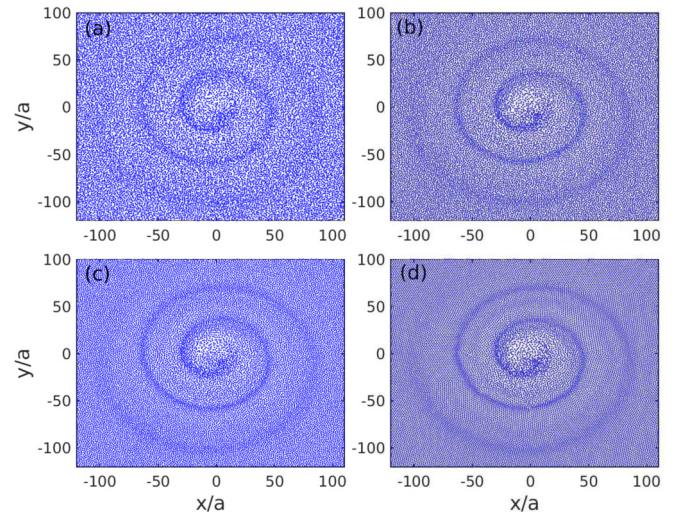


FIG. 7. Characteristics of a spiral wave with varying coupling parameters (a)  $\Gamma = 10$ , (b)  $\Gamma = 50$ , (c)  $\Gamma = 100$ , and (d)  $\Gamma = 800$ . The strength of REF, period of REF, and screening parameter for all the  $\Gamma$  are  $A = 0.203$ ,  $\omega_{pd}T_f = 26.88$ , and  $\kappa = 0.5$ , respectively. Snapshots of particles for all  $\Gamma$  are taken at time  $\omega_{pd}t = 71.68$ .

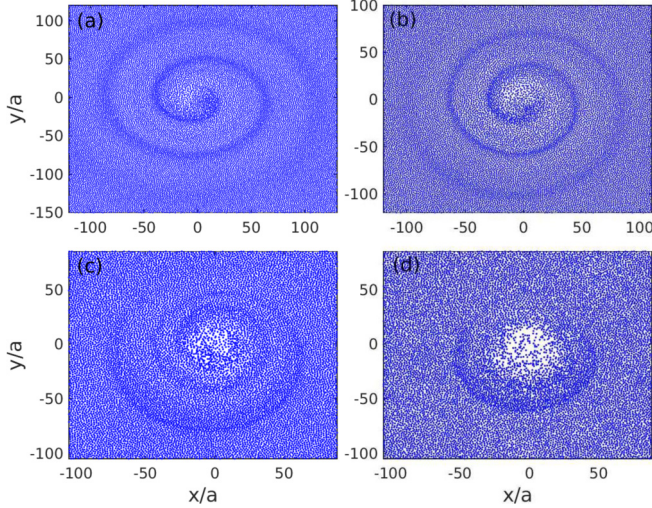


FIG. 8. The dynamics of spiral waves for different values of screening parameters (a)  $\kappa = 0.25$ , (b)  $\kappa = 0.50$ , (c)  $\kappa = 1.0$ , and (d)  $\kappa = 2.0$ . The amplitude of driver, period of driver, and coupling parameter for all the plots are  $A = 0.203$ ,  $\omega_{pd}T_f = 26.88$ , and  $\Gamma = 100$ , respectively. Snapshots of particles for all the  $\kappa$  are taken at time  $\omega_{pd}t = 71.68$ .

where

$$f(\kappa) = -0.0799 - 0.0046\kappa^2 + 0.0016\kappa^4.$$

The radial propagation speed decreases with increasing  $\kappa$ , so that for a given  $\kappa$  there is a critical frequency of the REF above which the disturbance gets smeared out instead of forming distinctly clear spiral rings [shown in plot (d) of Fig. 8]. It is thus clear that to form a proper unbroken spiral wave pattern, we require a proper combination of  $\omega_f$  and  $\kappa$  so that radial and angular velocities can appropriately compliment each other.

The increasing value of  $\kappa$  essentially implies that the interparticle shielding gets stronger and hence the individual dust particle interactions decrease. Due to the reduction in interparticle interaction, when the REF throws the particle out of the radial patch of forcing, the particles are unable to return back to their original location. Thus the particle density in the forcing region decreases. This is evident from Fig. 8, where one can easily notice [see the white patches in plots (c) and (d)] the reduction in particle number density in the central forcing region. As a result of this reduction in the number density, the subsequent rings of the spiral do not form clearly for high values of  $\kappa$ .

We have also investigated the possibility of exciting a spiral wave when the dust medium is initially in a crystalline phase. For this purpose, we have chosen the case of  $\Gamma = 2000$  for our studies. When the value of  $\kappa$  is small [plot (a) of Fig. 9], we observe the regular formation of a spiral wave. However, as  $\kappa$  is increased one observes that the spiral excitations have a hexagonal wavefront [plots (b), (c), and (d) of Fig. 9]. This observation can be understood by realizing that the original dust crystal lattice has hexagonal symmetry. When the value of  $\kappa$  is increased, interactions amidst particles get confined to a few nearest neighbors. In the hexagonal configuration, as shown in the schematic of Fig. 10, the nearest-neighbor distances along the lattice axis are smaller compared to those

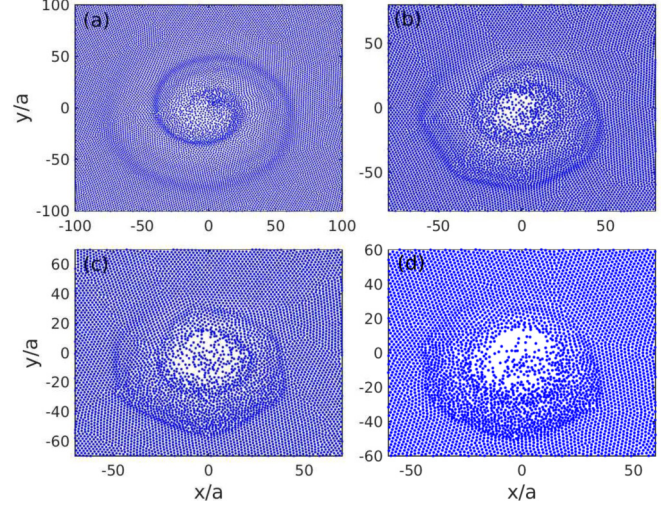


FIG. 9. Effect of screening parameters (a)  $\kappa = 0.5$ , (b)  $\kappa = 1.0$ , (c)  $\kappa = 1.5$ , and (d)  $\kappa = 2.0$  on the spiral structure when the dust medium is in a crystalline state. The amplitude of driver, period of driver, and coupling parameter for all the plots are  $A = 0.203$ ,  $\omega_{pd}T_f = 26.88$ , and  $\Gamma = 2000$ , respectively. Snapshots of particles for all  $\kappa$  are taken at time  $\omega_{pd}t = 53.76$ .

at the lattice diagonal. The asymmetry in the interparticle distance in the crystalline phase also influences the radial distribution function (RDF), which shows additional peaks in the distribution, as shown in Fig. 11. Furthermore, from Eq. (2), it is clear that the radial propagation speed depends on  $\kappa$  (the ratio of interparticle separation to Debye length). Thus the spiral disturbance propagates faster along the lattice axis (in this direction particles are aligned closer) and is slow along the lattice diagonal.

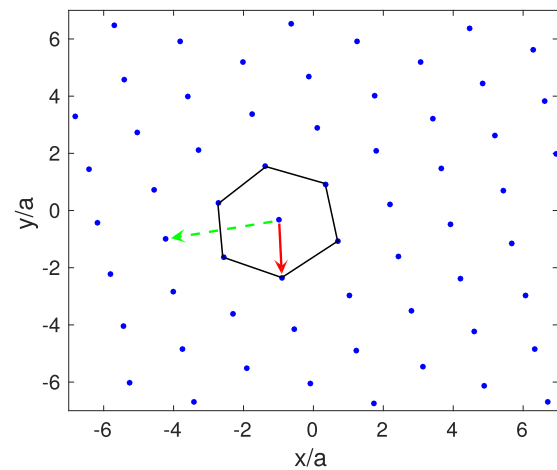


FIG. 10. Schematic representation of interparticle distance asymmetry when the dusty plasma is in a crystalline phase. This is the equilibrium snapshot of particles for  $\Gamma = 2000$  and  $\kappa = 1.5$ . Solid and dotted arrows depict the lattice axial and diagonal directions, respectively, in the crystal. The asymmetry in the dust crystal spacing has also been shown experimentally by Chu and Lin [41].

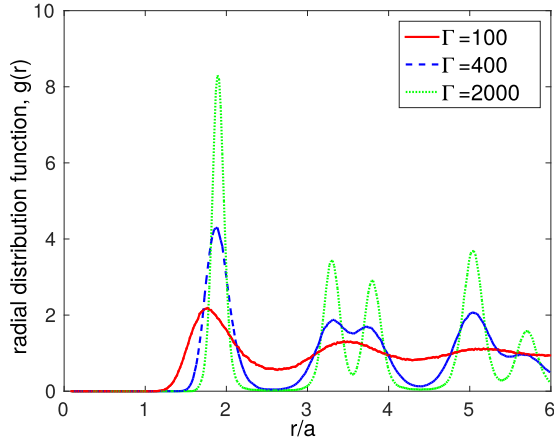


FIG. 11. Radial distribution functions (RDFs) for three  $\Gamma = 100$ , 400, and 2000 are shown here. The screening parameter ( $\kappa$ ) for all  $\Gamma$  is 1.5. At  $\Gamma = 2000$ , the appearance of one more peak near the second peak (the peak comes just after the sharp first peak) confirms the anisotropy in the interparticle distance of a hexagonal crystal.

#### IV. CONCLUSION

We have carried out MD simulations for a dusty plasma medium in the presence of forcing due to an external rotating electric field. We observe the formation of spiral waves. This indicates that the dusty plasma behaves like an excitable medium. The radial propagation is governed by the dust acoustic speed, and the rotation gets decided by the forcing period. The interplay between the two decides the spiral wave structure. For a distinctly clear spiral to form, a proper combination of the two is essential. In case the radial propagation is too slow, the rings diffuse among each other and the spiral structure is not so distinctive. The parametric dependence is consistent with the continuum study carried out by Kumar *et al.* [19] wherein the dusty plasma was considered as a viscoelastic fluid.

Further, we have shown that there are additional features that emerge when the discrete particle effects are taken into account using MD simulations. For instance, when the amplitude of forcing is high, the particles at the center get heated by acquiring random thermal velocity. This in turn effects the spacing of subsequent rings. Furthermore, a large amplitude forcing throws the particle out of the external forcing regime.

The restoring force to bring the particles back at the center would, however, depend on the interparticle interaction. When  $\kappa$  is chosen high, the shielding range is small and this restoring effect decreases. Thus for high amplitude and high  $\kappa$ , the central region where external forcing has been chosen to be finite becomes devoid of particles. The spiral then fails to form adequately.

Another interesting feature that has been observed is when the dust medium is in a 2D hexagonal crystalline state. In this case, for high values of  $\kappa$  (for which the interparticle potential gets very weak) only a few neighboring particles participate in interactions. The spiral waveform in such cases has a hexagonal front. This can be understood by realizing that for a hexagonal lattice, the nearest-neighbor separation along different directions varies, as has been illustrated by the schematic of Fig. 10. Thus, there is an anisotropy in the medium, and the radial propagation speed will depend on the strength of the nearest-neighbor interaction.

It is our firm belief that spiral waves as observed in our simulation could also be observed in experiments related to systems such as dusty plasmas, e-i plasmas, colloids, and condensed matter. There have been recent dusty plasma experiments in which rotating electric fields of the kind used in this paper were applied over the entire system [33,34]. However, it can be quite challenging to have the force in a limited region of the experiment, as is desired for the spiral wave excitations. We feel that one possible solution could be to insert a probe that bifurcates as a tuning fork at its other end. A potential difference can then be applied between the two prongs of the fork. The rest of the structure can be insulated. This fork can then be rotated mechanically in time. This will produce an electric field over a rectangular strip that spans a circular region with time and serving as REF. For ease of numerics, we had chosen a fixed circular patch region where the REF was finite all throughout time. However, we feel that the experimentalists will be in a better position to improvise and come up with an appropriate solution for this particular requirement.

#### ACKNOWLEDGMENTS

We would like to gratefully acknowledge the late P. K. Kaw for enlightening discussions.

- 
- [1] J. J. Tyson and J. P. Keener, *Physica D* **32**, 327 (1988).
  - [2] *Nonlinear Wave Processes in Excitable Media*, Vol. 244 of NATO Advanced Study Institute Series B: Physics, edited by A. V. Holden, M. Markus, and H. G. Othmer (Plenum Press, New York, 1991).
  - [3] V. S. Zykov and E. Bodenschatz, *Annu. Rev. Condens. Matter Phys.* **9**, 435 (2018).
  - [4] J. Keener and J. Tyson, *Physica D* **21**, 307 (1986).
  - [5] V. Perez-Muñuzuri, R. Aliev, B. Vasiev, V. Perez-Villar, and V. I. Krinsky, *Nature (London)* **353**, 740 (1991).
  - [6] X. Huang, W. Xu, J. Liang, K. Takagaki, X. Gao, and J. Young Wu, *Neuron* **68**, 978 (2010).
  - [7] G. Bub, A. Shrier, and L. Glass, *Phys. Rev. Lett.* **88**, 058101 (2002).
  - [8] R. FitzHugh, *Biophys. J.* **1**, 445 (1961).
  - [9] J. Nagumo, S. Arimoto, and S. Yoshizawa, *Proc. IRE* **50**, 2061 (1962).
  - [10] D. Barkley, M. Kness, and L. S. Tuckerman, *Phys. Rev. A* **42**, 2489 (1990).
  - [11] A. Pertsov, E. Ermakova, and A. Panfilov, *Physica D* **14**, 117 (1984).
  - [12] T. Frisch, S. Rica, P. Coulet, and J. M. Gilli, *Phys. Rev. Lett.* **72**, 1471 (1994).
  - [13] D. M. Elmegreen, *Astrophys. J. Suppl. Ser.* **47**, 229 (1981).
  - [14] V. Springel and L. Hernquist, *Astrophys. J. Lett.* **622**, L9 (2005).
  - [15] E. A. Martens, C. R. Laing, and S. H. Strogatz, *Phys. Rev. Lett.* **104**, 044101 (2010).
  - [16] S.-I. Shima and Y. Kuramoto, *Phys. Rev. E* **69**, 036213 (2004).

- [17] G.-Q. Sun, Z. Jin, Q.-X. Liu, and L. Li, *J. Stat. Mech.: Theor. Exp.* (2008) P08011.
- [18] L. Li, X. Liao, K. H. Chan, and K. Zhang, *Phys. Fluids* **22**, 011701 (2010).
- [19] S. Kumar, B. Patel, and A. Das, *Phys. Plasmas* **25**, 043701 (2018).
- [20] U. Konopka, G. E. Morfill, and L. Ratke, *Phys. Rev. Lett.* **84**, 891 (2000).
- [21] T. Palberg, W. Mönch, F. Bitzer, R. Piazza, and T. Bellini, *Phys. Rev. Lett.* **74**, 4555 (1995).
- [22] T. Terao and T. Nakayama, *Phys. Rev. E* **60**, 7157 (1999).
- [23] Y. Levin, *Rep. Prog. Phys.* **65**, 1577 (2002).
- [24] A. A. Lee, C. S. Perez-Martinez, A. M. Smith, and S. Perkin, *Phys. Rev. Lett.* **119**, 026002 (2017).
- [25] M. Lyon, S. D. Bergeson, and M. S. Murillo, *Phys. Rev. E* **87**, 033101 (2013).
- [26] C. E. Simien, Y. C. Chen, P. Gupta, S. Laha, Y. N. Martinez, P. G. Mickelson, S. B. Nagel, and T. C. Killian, *Phys. Rev. Lett.* **92**, 143001 (2004).
- [27] P. Hartmann, G. J. Kalman, Z. Donkó, and K. Kutasi, *Phys. Rev. E* **72**, 026409 (2005).
- [28] S. Kumar, S. K. Tiwari, and A. Das, *Phys. Plasmas* **24**, 033711 (2017).
- [29] M. Tribeche and A. Merriche, *Phys. Plasmas* **18**, 034502 (2011).
- [30] D. Samsonov, S. K. Zhdanov, R. A. Quinn, S. I. Popel, and G. E. Morfill, *Phys. Rev. Lett.* **92**, 255004 (2004).
- [31] M. Choudhary, S. Mukherjee, and P. Bandyopadhyay, *Phys. Plasmas* **24**, 033703 (2017).
- [32] M. R. Akdim and W. J. Goedheer, *Phys. Rev. E* **67**, 056405 (2003).
- [33] V. Nosenko, A. V. Ivlev, S. K. Zhdanov, M. Fink, and G. E. Morfill, *Phys. Plasmas* **16**, 083708 (2009).
- [34] L. Wörner, V. Nosenko, A. V. Ivlev, S. K. Zhdanov, H. M. Thomas, G. E. Morfill, M. Kroll, J. Schablinski, and D. Block, *Phys. Plasmas* **18**, 063706 (2011).
- [35] S. Plimpton, *J. Comput. Phys.* **117**, 1 (1995).
- [36] V. Nosenko and J. Goree, *Phys. Rev. Lett.* **93**, 155004 (2004).
- [37] S. Nosé, *Mol. Phys.* **52**, 255 (1984).
- [38] W. G. Hoover, *Phys. Rev. A* **31**, 1695 (1985).
- [39] M. Schwabe and D. B. Graves, *Phys. Rev. E* **88**, 023101 (2013).
- [40] B. Liu and J. Goree, *Phys. Plasmas* **24**, 103702 (2017).
- [41] J. H. Chu and L. I., *Phys. Rev. Lett.* **72**, 4009 (1994).
- [42] S. A. Khrapak and H. M. Thomas, *Phys. Rev. E* **91**, 033110 (2015).
- [43] G. Kalman, M. Rosenberg, and H. E. DeWitt, *Phys. Rev. Lett.* **84**, 6030 (2000).